hydrogen

MDPI

Article

Effect of Na^+ vs. K^+ Cations and Carbonate Presence on Urea Oxidation Reaction Coupled with Green Hydrogen Production in Alkaline Media: A Voltammetric and Electrochemical Impedance Spectroscopy Study

Vyacheslav S. Protsenko [1,2,*], Denys A. Shaiderov [2] and Oleksandr D. Sukhatskyi [1,2]

[1] Department of Physical Chemistry, Ukrainian State University of Science and Technologies, Lazaryan St. 2, 49010 Dnipro, Ukraine
[2] Research Institute of Electroplating and Chemistry, Ukrainian State University of Science and Technologies, Lazaryan St. 2, 49010 Dnipro, Ukraine
* Correspondence: vprotsenko7@gmail.com

Abstract

This work reports the electrochemical behavior of a nickel hydroxide electrode, electrodeposited in a deep eutectic solvent (DES), in alkaline solutions of varying composition, aiming to elucidate the influence of the cation (Na^+ vs. K^+), urea, and carbonate ions on the mechanism and kinetics of anodic processes. Cyclic voltammetry and electrochemical impedance spectroscopy were employed to analyze the electrochemical responses of electrode processes in alkaline water electrolysis systems. For the urea oxidation reaction (UOR), the frequency-dependent characteristics were thoroughly characterized, and the impedance response was simulated according to the Armstrong–Henderson equivalent circuit. It was found that the addition of urea significantly transforms the impedance structure, sharply reducing the polarization resistance and increasing the pseudo-capacitive component of the constant phase element at low frequencies, indicating activation of the slow steps of urea oxidation via a direct mechanism and the formation of an extended adsorptive surface. It was demonstrated that, unlike conventional alkaline electrolysis where KOH-based systems are generally more effective, urea-assisted systems exhibit superior performance in NaOH-based electrolytes, which provides more favorable kinetics for the electrocatalytic urea oxidation process. Furthermore, the accumulation of carbonate ions was shown to negatively affect UOR kinetics by increasing polarization resistance and partially blocking surface sites, highlighting the necessity of controlling electrolyte composition in practical systems. These findings open new opportunities for the rational design of efficient urea-assisted electrolyzers for green hydrogen generation.

Keywords: green hydrogen production; urea oxidation reaction; electrochemical impedance; electrocatalysis; alkaline water electrolysis

Academic Editor: Silvano Tosti

Received: 25 November 2025
Revised: 6 December 2025
Accepted: 12 December 2025
Published: 14 December 2025

Citation: Protsenko, V.S.; Shaiderov, D.A.; Sukhatskyi, O.D. Effect of Na^+ vs. K^+ Cations and Carbonate Presence on Urea Oxidation Reaction Coupled with Green Hydrogen Production in Alkaline Media: A Voltammetric and Electrochemical Impedance Spectroscopy Study. *Hydrogen* **2025**, *6*, 119. https://doi.org/10.3390/hydrogen6040119

1. Introduction

Hydrogen is currently considered the most promising energy carrier both at present and in the future, as its use as a fuel meets strict environmental requirements and helps prevent the intensification of the greenhouse effect on Earth caused by widespread fossil fuel consumption [1,2]. Hydrogen is increasingly recognized as a key clean energy vector capable of supporting large-scale decarbonization across multiple sectors. Recent analyses

highlight its role in long-term renewable energy storage, its integration with intermittent solar and wind power, and its potential to replace fossil-fuel-based technologies in transport and industry [3]. In this context, it is important to emphasize the notable progress in methods for sustainable hydrogen production from eco-friendly resources [4], including hydrogen generation via dehydrogenation of organic molecules [5,6], solar-driven H_2 production using semiconductor heterojunctions [7–9], and the use of biomass-derived molecules as renewable electron donors [10–12], many of which have demonstrated high efficiencies under solar irradiation.

Despite rapid developments in photocatalytic and thermochemical H_2-generation technologies, alkaline electrolysis remains the most mature and widely implemented method because of its proven reliability, scalability, ability to operate steadily independent of solar conditions, and the availability of low-cost, durable electrode materials [13]. Water electrolysis powered by renewable energy sources such as solar, wind, or hydropower is therefore widely regarded as the cleanest pathway for hydrogen production [14–16]. Hydrogen produced in this way is referred to as green hydrogen [14]. However, the electrochemical synthesis of green hydrogen, which relies on the implementation of cathodic hydrogen evolution reaction (HER) (1) and anodic oxygen evolution reaction (OER) (2), also has several drawbacks. Among the most significant is the relatively high energy consumption, which is due to the substantial difference in the thermodynamic electrode potentials of reactions (1) and (2), amounting to 1.23 V at 298 K [14].

$$2H_2O + 2e^- \rightarrow H_2 + 2OH^-,\ E^0 = -0.83\ V \quad (1)$$

$$4OH^- \rightarrow O_2 + 2H_2O + 4e^-,\ E^0 = 0.40\ V \quad (2)$$

An effective approach to reducing energy consumption in water electrolysis is to replace the anodic oxygen evolution reaction (2) with an alternative, less energy-demanding process involving various organic and inorganic compounds [17]. In particular, one of the most attractive options is the replacement of the oxygen evolution reaction with the urea oxidation reaction (UOR) (3), which is favored due to a combination of economic, environmental, and technological factors [18–24].

$$CO(NH_2)_2(aq) + 8OH^- \rightarrow N_2(g) + 6H_2O + CO_3^{2-}(aq) + 6e^- \quad (3)$$

Although urea is often discussed in the context of wastewater contamination [25], it is also an essential industrial chemical widely used in fertilizer production [26], resin synthesis [27], pharmaceuticals [28], and other chemical processes. This dual role explains the growing interest in technologies that enable both its removal and valorization through electrochemical conversion.

The advantages of green hydrogen production via the UOR include the wide availability, non-toxicity, and low cost of urea. Moreover, the thermodynamically favorable nature of the process (according to recent refined calculations, the thermodynamic potential of reaction (3) is –0.852 V [29,30]) indicates the exceptional suitability of this reaction as a potential replacement for reaction (2) from the perspective of core green chemistry principles [31]. In addition, the alkaline medium prevents the release of carbon dioxide as a final product into the atmosphere, with carbon remaining in solution as carbonate ions, thereby avoiding a carbon footprint.

However, the kinetics of the multi-electron transfer in reaction (3) is sluggish [21,22]. Therefore, it is not surprising that considerable attention in urea-assisted water splitting processes is devoted to the development of new highly efficient electrocatalysts with enhanced activity and stability [19–22,32]. Nevertheless, the efficiency of electrochemical

green hydrogen synthesis is determined not only by the characteristics of the electrocatalyst itself but also by the properties of the electrolyte solution used in electrolysis, whose composition and component concentrations can, in principle, be varied within certain limits. In particular, for alkaline water electrolysis, solutions of either NaOH or KOH can be alternatively employed. Moreover, during the implementation of the anodic reaction (3), carbonate ions may gradually accumulate in the solution, which can also influence electrode polarization. The effects of these factors on urea-assisted water electrolysis remain largely unexplored. Therefore, the aim of this work was to evaluate: (1) the influence of the cation nature (Na^+ or K^+) and (2) the effect of carbonate ion addition on the electrochemical urea oxidation reaction in aqueous alkaline media. Both cyclic voltammetry and electrochemical impedance spectroscopy were employed for this purpose. As the electrocatalyst, a nickel hydroxide-based coating electrodeposited from a solution of a deep eutectic solvent (DES, a new generation of ionic liquids) was used [33]. As is well known, DESs, due to a number of environmental and technological advantages, have recently attracted considerable attention in the development of novel electrocatalysts [34–39].

2. Materials and Methods

The $Ni(OH)_2$-based coating used as the electrocatalyst in this study was prepared following the same electrodeposition procedure described in detail in our previous publication [33], employing identical plating bath composition and deposition parameters. Structural and morphological characterization of this deposition protocol (XRD, SEM, and EDX) was reported in ref. [33] and revealed a predominantly $Ni(OH)_2$ phase with uniform nanostructured morphology and good adhesion to the substrate; therefore, these results are taken as the reference characterization for the material used in the present work.

The deep eutectic solvent, known as *ethaline*, was prepared by thoroughly mixing crystalline choline chloride (99%, Acros Organics; CAS 67-48-1) and ethylene glycol (>99%, Sigma-Aldrich; CAS 107-21-1) at a molar ratio of 33.33% to 66.67%, respectively. This liquid eutectic mixture was intensively stirred on a magnetic stirrer at approximately 70 °C for several hours until complete homogenization was achieved. A weighed amount of solid $NiCl_2 \cdot 6H_2O$ (>99%, Sigma-Aldrich; CAS 7791-20-0) was then dissolved in the prepared ethaline to obtain a solution containing 0.25 mol dm^{-3} of Ni(II) ions. The resulting electrolyte for electrocatalyst deposition was stored in a desiccator in the presence of pre-dried calcium chloride to prevent the absorption of atmospheric moisture. The residual water content in the electrolyte, determined using the Karl Fischer method, did not exceed 1%.

Electrodeposition was carried out on the surface of a disc-shaped polished platinum electrode with a diameter of 5 mm embedded in a glass holder. The electrocatalyst was prepared using a specially developed procedure to ensure the formation of a uniform layer with satisfactory adhesion to the platinum substrate. For this purpose, the platinum surface was first etched in an aqueous HCl solution (1:1 v/v) at approximately 40–50 °C for 5 min. After thorough rinsing with distilled water and drying with a warm air stream, the Pt electrode was anodically treated in a galvanostatic mode in an H_2SO_4 solution (1:1 v/v) at approximately 25 °C for 5 min at an anodic current density of 40 mA cm^{-2}, using another platinum electrode as the cathode. The platinum surface was then rinsed with distilled water, dried with warm air, and subsequently cathodically treated in a galvanostatic mode in a 1 M NaOH solution at approximately 25 °C for 5 min at a current density of 20 mA cm^{-2}, using another platinum electrode as the anode. After this treatment, the surface was again thoroughly rinsed with distilled water, dried with a warm air stream, and immediately used for electrodeposition of the coating from the DES-based electrolyte.

Electrodeposition was performed under constant-current conditions using a stabilized power supply (Electronics 30V 6A) in a thermostated glass cell maintained at 50 ± 0.01 °C.

Deposition was carried out at a cathodic current density of 10 mA cm^{-2} with continuous electrolyte stirring using a magnetic stirrer at 500 rpm for 2 h [33].

The freshly deposited coating was thoroughly rinsed with a stream of distilled water, dried in a flow of cold air, and immediately used for evaluating its electrocatalytic properties.

To assess the influence of the alkali cation (Na^+ or K^+) and the presence of carbonate ions in the alkaline media on the electrocatalytic behavior of the DES-derived coating, deaerated aqueous alkaline solutions of the following compositions were used:

(1) 1 M NaOH;
(2) 1 M KOH;
(3) 1 M NaOH + 0.1 M Na_2CO_3;
(4) 1 M KOH + 0.1 M K_2CO_3;
(5) 1 M NaOH + 0.33 M $CO(NH_2)_2$;
(6) 1 M KOH + 0.33 M $CO(NH_2)_2$;
(7) 1 M NaOH + 0.33 M $CO(NH_2)_2$ + 0.1 M Na_2CO_3;
(8) 1 M KOH + 0.33 M $CO(NH_2)_2$ + 0.1 M K_2CO_3.

Experiments were carried out in a thermostated glass cell at 25 ± 0.01 °C using a three-electrode configuration. The coating deposited on the platinum substrate served as the working electrode. A platinum mesh with a geometric area much larger than that of the working electrode was used as the counter electrode. A saturated Ag/AgCl electrode served as the reference.

Polarization of the working electrode for cyclic voltammetry and electrochemical impedance spectroscopy was performed using a Reference 3000 potentiostat (Gamry). In the cyclic voltammetry experiments, the electrode surface was first pre-treated by polarizing it at –1.5 V for 2 min in the alkaline medium. This step was accompanied by intense hydrogen evolution, ensuring high reproducibility of electrochemical measurements. After this pre-treatment, the potential was scanned linearly in the anodic direction up to +1.5 V, after which the scan direction was reversed toward more negative potentials down to −1.5 V. Without interrupting the polarization, the next scan was immediately initiated, following the same potential-sweep program. This surface-conditioning approach, developed and described in our previous publication [33], produced stabilized voltammograms after approximately 5–6 cycles, at which point a noticeable hysteresis was observed, most likely due to progressive changes in the state of the electrode surface. The cyclic voltammograms (CVAs) presented below correspond to the eleventh scan, where their shape becomes essentially invariant from one cycle to the next. The potential scan rate was 50 mV s^{-1}. In these experiments, the ohmic contribution was measured and compensated using the potentiostat's built-in iR compensation function.

Immediately after recording the eleventh potential sweep, without removing the working electrode from the alkaline solution, the electrochemical impedance measurement program was initiated. This approach ensured good reproducibility of the obtained impedance spectra. Electrochemical impedance was measured in the potentiostatic mode. The amplitude of the sinusoidal potential perturbation was 5 mV. Measurements were performed in the frequency range from 100 kHz to 0.01 Hz. The acquired data were processed, and the parameters of the selected equivalent circuit were determined using the licensed Echem Analyst™ Software, version 5.6 (Gamry Instruments, Warminster, PA, USA).

3. Results and Discussion

Before analyzing the electrochemical data, it is appropriate to note that, according to previously published findings [33], the as-deposited electrocatalytic coating used in this study consists predominantly of the β-$Ni(OH)_2$ phase. It is also worth recalling that the high electrocatalytic activity of nickel hydroxide toward the urea oxidation reaction has

long been recognized [18–22], and its catalytic action is commonly interpreted in terms of two possible reaction pathways, referred to as the *direct* and *indirect mechanisms* [40–44]. According to the direct mechanism (Equations (4) and (5)), adsorbed urea molecules located at the active NiOOH sites interact with hydroxide ions, either those adsorbed on the electrocatalyst surface or those originating from the bulk alkaline solution, to form the final oxidation products. The active NiOOH sites are generated through the prior oxidation of $Ni(OH)_2$ (reaction (4)).

$$Ni(OH)_2 + OH^- \rightarrow NiOOH + H_2O + e^- \quad (4)$$

$$CO(NH_2)_2 + 6OH^- \xrightarrow{NiOOH} N_2 + CO_2 + 5H_2O + 6e^- \quad (5)$$

The indirect mechanism assumes that NiOOH chemically oxidizes the adsorbed $CO(NH_2)_2$ molecules (Equation (6)), while the active NiOOH sites on the surface are regenerated through reaction (4).

$$6NiOOH + CO(NH_2)_2 + H_2O \rightarrow 6Ni(OH)_2 + N_2 + CO_2 \quad (6)$$

Thus, in the direct mechanism, urea oxidation proceeds directly through the electrochemical step (5), whereas in the indirect mechanism it occurs via the chemical interaction described by reaction (6). Both the direct and indirect pathways may operate simultaneously on the electrode surface [44].

Figure 1 shows paired cyclic voltammograms (CVAs) recorded in the investigated alkaline solutions, both in the presence and absence of urea, with varying contents of inorganic components. In Figure 2, for ease of comparison, the same curves are presented separately, grouped for solutions without $CO(NH_2)_2$ (Figure 2a) and with its presence (Figure 2b).

The cyclic voltammograms registered in alkaline solutions without urea exhibit several characteristic regions corresponding to specific electrochemical transformations. The cathodic region at E < –1.0 V corresponds to the hydrogen evolution reaction, while the anodic region at E > ≈0.7 V corresponds to the oxygen evolution reaction. The cathodic-anodic waves observed in the CVAs between approximately +0.2 and +0.7 V are known to be associated with the electrochemical transformations of the Ni(II)↔Ni(III) redox couple [18,33,40,41], which, in a first approximation, are represented by Equation (4). In alkaline electrolytes containing dissolved urea, the UOR begins at electrode potentials greater than approximately 0.2–0.5 V.

It should be noted that the recorded CVAs exhibit virtually no noticeable hysteresis between the forward and reverse (anodic and cathodic) scans, apparently due to the surface-preparation procedure described above, which ensures sufficient stability of the electrocatalytic activity over a prolonged period [33]. Noticeable hysteresis is observed only in the region corresponding to the urea oxidation reaction, likely as a result of certain diffusion limitations in the transport of $CO(NH_2)_2$ molecules and some evolution in the state of the electrocatalyst surface.

Next, it is appropriate to briefly describe the influence of the electrolyte composition on the kinetics of these main individual electrochemical processes in urea-assisted hydrogen production.

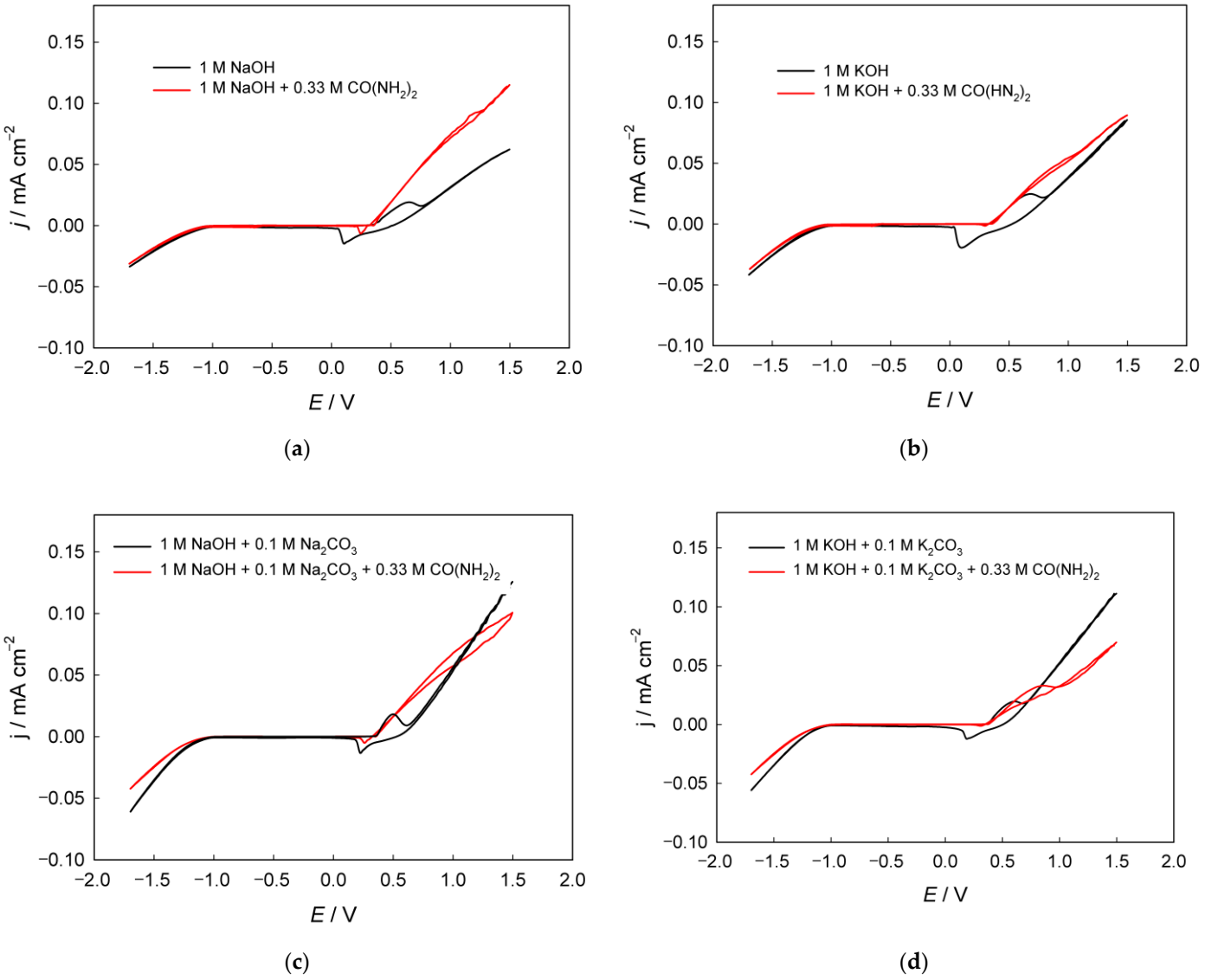

Figure 1. CVAs recorded in solutions of different compositions (as indicated in the figure): (**a**,**c**) NaOH-based solutions; (**b**,**d**) KOH-based solutions.

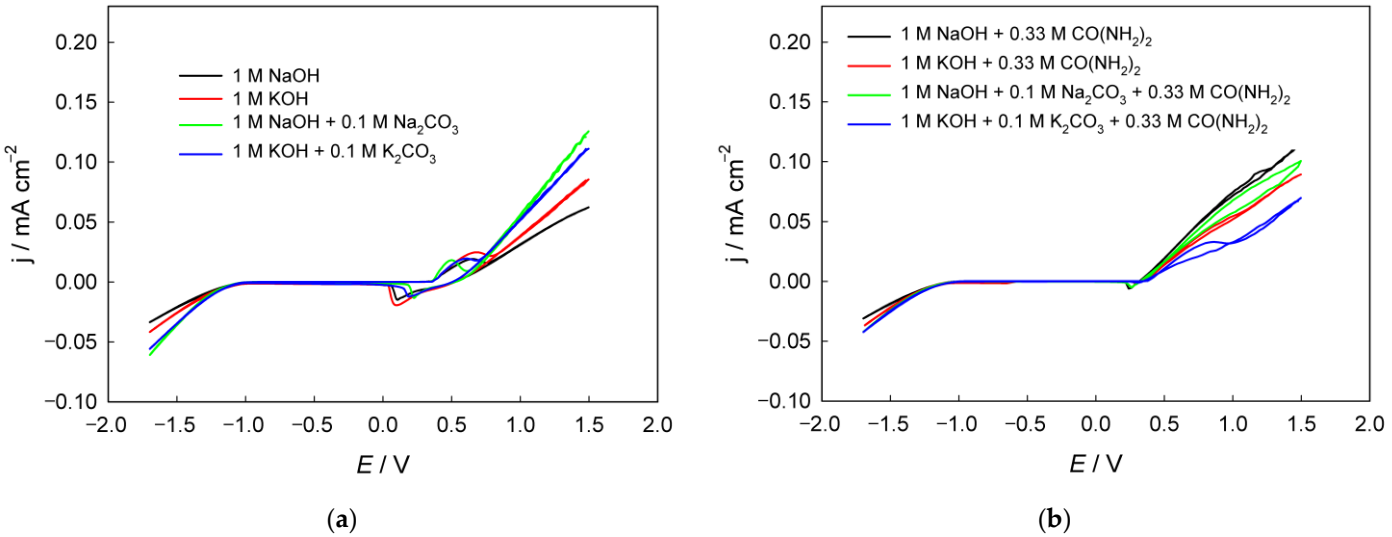

Figure 2. CVAs recorded in solutions of different compositions: (**a**) without added urea; (**b**) with urea added to the solution.

(1) Hydrogen evolution reaction

Comparison of the cathodic regions in Figure 2a indicates that the polarization of the hydrogen evolution reaction in 1 M KOH is lower than in 1 M NaOH. This effect can be explained by the weaker hydration of K^+ ions compared to Na^+ ions, which facilitates the discharge of water molecules and the subsequent formation of adsorbed hydrogen atoms on the cathode surface [45]. In addition, the less ordered hydration shell of K^+ ions leads to the formation of a thinner electrical double layer and increases the activity of water molecules near the electrode–solution interface, thereby accelerating the kinetics of the hydrogen evolution reaction. Similar patterns have been reported previously in several studies, confirming that the HER overpotential decreases in the series LiOH > NaOH > KOH under comparable conditions [45–47].

The experimental results also indicate that the addition of sodium or potassium carbonate to 1 M NaOH or 1 M KOH solutions, respectively, significantly reduces the polarization of the HER (Figure 1c,d). This effect can be associated with the specific influence of carbonate ions on the structure of interfacial water and the electrical double layer. The presence of CO_3^{2-} ions weakens the hydration of alkali cations, increases the activity of water molecules near the electrode surface, and facilitates the Volmer discharge step. In addition, the CO_3^{2-}/HCO_3^- equilibrium acts as a local buffer, stabilizing the interfacial pH and promoting more efficient hydrogen evolution, which is attributed to an additional pathway of HER, namely bicarbonate-mediated reduction [48].

The presence of urea in alkaline electrolyte inhibits the hydrogen evolution reaction (Figure 1). This inhibition may originate from molecular adsorption of urea on the electrode surface, which blocks active sites and alters the interfacial water structure [49,50]. The hydrogen-bonding interaction between urea and water decreases the activity of water molecules and hinders the Volmer step. Moreover, urea may modify the electrical double layer and increases the charge-transfer resistance, leading to a higher HER overpotential.

(2) Oxygen evolution reaction

The oxygen evolution reaction on nickel hydroxide-based electrodes typically proceeds with lower polarization in 1 M KOH compared to 1 M NaOH (Figure 2). Similarly to the HER, this effect is primarily attributed to the weaker hydration and higher mobility of K^+ ions relative to Na^+, which facilitate the interfacial transport of hydroxide ions and improve charge transfer kinetics at the NiOOH/electrolyte interface. Moreover, the larger ionic radius of K^+ results in a less compact interfacial double layer and a weaker local electric field, both of which promote the formation and stabilization of active NiOOH species. This effect of the alkali-metal ion nature on alkaline oxygen evolution has already been described in the literature [51–53].

The addition of carbonate ions to alkaline electrolytes such as 1 M KOH or 1 M NaOH markedly decreases the polarization of the oxygen evolution reaction on electrodes under study. This effect can be explained by several interrelated factors. First, the CO_3^{2-}/HCO_3^- equilibrium provides a buffering effect that maintains a high local hydroxide ion concentration near the electrode surface, thus facilitating charge transfer. Second, carbonate ions can weakly adsorb on NiOOH surfaces, altering the interfacial electric field and stabilizing highvalent Ni^{3+}/Ni^{4+} species that serve as the active centers for the OER. In addition, the presence of carbonate ions disrupts the strong hydration shells of alkali cations, improving the mobility of charge carriers and decreasing the interfacial resistance. Previously, it was noted [54] that anions in the electrical double layer can disrupt the water network at the interface, thereby affecting the kinetics of oxygen evolution at the anode. These combined physicochemical effects lead to significantly enhanced OER kinetics in carbonate-containing alkaline solutions.

(3) $Ni(OH)_2$/NiOOH redox reaction

As mentioned above, the cathodic–anodic waves at electrode potentials of approximately +0.2 . . . +0.7 V in alkaline media are associated with the redox transformation of reaction (4). The data show that the amount of charge consumed in these processes, as indicated by the area under the voltammetric curve, slightly increases when moving from NaOH to KOH solution. This effect can be attributed to the specific influence of K^+ cations on the electrochemical behavior of nickel hydroxide. Potassium cations with lower hydration energy are more easily adsorbed or possibly partially intercalated into the layered structure of NiOOH, stabilizing a phase with a larger interlayer spacing and promoting the participation of a greater number of Ni-containing sites in the redox processes. As a result, this causes an increase in the integral charge under the voltammetric peaks, i.e., the growth of the capacitance of the nickel-hydroxide electrode [52].

Regarding the addition of carbonate ions to the alkaline solution, Figure 2a shows that this decreases the potential difference between the cathodic and anodic peaks, indicating enhanced electrochemical reversibility of the process for both NaOH and KOH. This behavior can be explained by the specific interaction of carbonate anions with the layered $Ni(OH)_2$/NiOOH structures. Carbonate ions may adsorb or intercalate into the interlayer space of nickel hydroxides, stabilizing γ-type or mixed (α/γ) phases with larger interlayer spacing [55,56]. Simultaneously, the CO_3^{2-}/HCO_3^- buffering system reduces pH fluctuations in the near-electrode region, promoting greater structural stability and increasing the reversibility of the $Ni(OH)_2 \leftrightarrow$ NiOOH redox transformation.

(4) Urea oxidation reaction

The data in Figure 1 confirm numerous observations repeatedly reported in the literature [18–23,32,33,43,44,57] that in alkaline solution, in the presence of added urea, the anodic current significantly increases immediately upon the formation potential of NiOOH being reached. Importantly, the recorded currents substantially exceed the corresponding peak currents of NiOOH formation in solutions without $CO(NH_2)_2$. This indicates a clear electrocatalytic effect in the urea oxidation reaction, proceeding according to Equations (5) and/or (6). It should be observed that the cathodic peak of the NiOOH reduction to $Ni(OH)_2$ is noticeably smaller than in solutions without urea, which likely indicates partial consumption of NiOOH via the indirect mechanism.

The anodic portion of the CVAs corresponding to the UOR is significantly shifted to more negative potentials compared to the OER on the same catalyst in the same solution but without added urea. For example, in 1 M NaOH solution, at a current density of 0.05 mA cm^{-2}, the oxygen evolution potential is approximately 1.27 V, whereas after adding 0.33 M $CO(NH_2)_2$, it decreases to 0.77 V, indicating a pronounced depolarization due to the replacement of the OER by UOR. This conclusion holds true for alkaline solutions regardless of the nature of the alkali metal cation (Na^+/K^+) and regardless of the presence of added carbonate ions. Thus, the possibility of significantly reducing the energy consumption of the anodic process is confirmed when using urea-assisted alkaline water electrolysis on the investigated nickel-containing electrocatalyst obtained via electrodeposition from a DES.

The pronounced hysteresis of the reverse CVA scan (in the cathodic direction corresponding to the UOR) at sufficiently high current densities is likely associated both with the evolution of the concentration and activity of the active sites during the reaction under potential scanning conditions and with the diffusion limitations of urea mass transport. Therefore, the electrocatalytic effect is most appropriately and accurately evaluated and compared for solutions of different compositions at relatively low urea oxidation current densities, where hysteresis effects in the forward and reverse CVA scans are practically absent. Accordingly, Table 1 summarizes the urea oxidation current densities in solutions of different compositions at a potential of +0.45 V, chosen near the foot of the current wave,

where mass transport limitations are expected to be minimal. Two important conclusions can be drawn from these data, both for theory and practical applications: (1) the electrocatalytic urea oxidation proceeds at a higher rate (i.e., higher anodic current density at a fixed potential) in NaOH-based solutions compared to KOH-based solutions under otherwise identical conditions; and (2) the presence of additional carbonate ions in the solution slightly hinders the urea oxidation process, as evidenced by lower observed current densities.

Table 1. Anodic urea oxidation current densities measured in solutions of different compositions at an electrode potential of +0.45 V.

Electrolyte Composition	j/mA cm^{-2}
1 M NaOH + 0.33 M $CO(NH_2)_2$	0.014
1 M KOH + 0.33 M $CO(NH_2)_2$	0.010
1 M NaOH + 0.33 M $CO(NH_2)_2$ + 0.1 M Na_2CO_3	0.012
1 M KOH + 0.33 M $CO(NH_2)_2$ + 0.1 M K_2CO_3	0.006

To explain the observed effects and gain a deeper understanding of the kinetics and mechanism of the urea electrooxidation reaction in solutions of different compositions, electrochemical impedance spectroscopy (EIS) was carried out. Impedance measurements were performed at a potential of +0.45 V, which, as noted above, allows for a correct assessment of the electrocatalytic activity and avoids complications arising from possible mass transport limitations.

As seen in Figure 3, the recorded Nyquist plots consist of a combination of two distorted (compressed) semicircles in the high- and low-frequency regions in alkaline solutions both without and with added urea. The semicircles in the Nyquist plots for solutions without $CO(NH_2)_2$ differ significantly in diameter: the high-frequency semicircle (i.e., the left semicircle in the plots) has a substantially smaller diameter than the low-frequency one (i.e., the right semicircle in the plots), which is highlighted in the inset of Figure 3. As is well known, the presence of a semicircle in a Nyquist plot indicates a certain time constant, which generally corresponds to the slowed charge transfer of a particular electrochemical step, and the larger the semicircle diameter, the higher the electrode resistance to the current of the electrochemical reaction [58,59]. The high-frequency semicircle (on the left of the Nyquist plot) can likely be attributed to the charge transfer associated with the $Ni(OH)_2 \leftrightarrow$ NiOOH redox conversion [44]. On this semicircle, the point corresponding to the maximum value of the imaginary component of the complex impedance, known as the characteristic frequency f_{peak}, can be clearly identified [58]. Then, the time constant, τ, associated with this semicircle can be calculated using the following Equation:

$$\tau = \frac{1}{2\pi f_{peak}} \quad (7)$$

The characteristic frequencies and the corresponding calculated time constants for the high-frequency semicircle in the Nyquist plots of alkaline solutions are summarized in Table 2. As follows from the obtained data, switching from NaOH to KOH results in a slight increase in the time constant, with characteristic frequencies of several hertz. The addition of carbonate salts to the respective alkalis leads to a noticeable decrease in the time constant, with characteristic frequencies approaching ~70–100 Hz. When urea is added to the solution, the time constants in the high-frequency region for different solution compositions become leveled, being approximately $\approx$(1–2) $\times$ 10^{-2} s at the corresponding characteristic frequencies of 7–16 Hz.

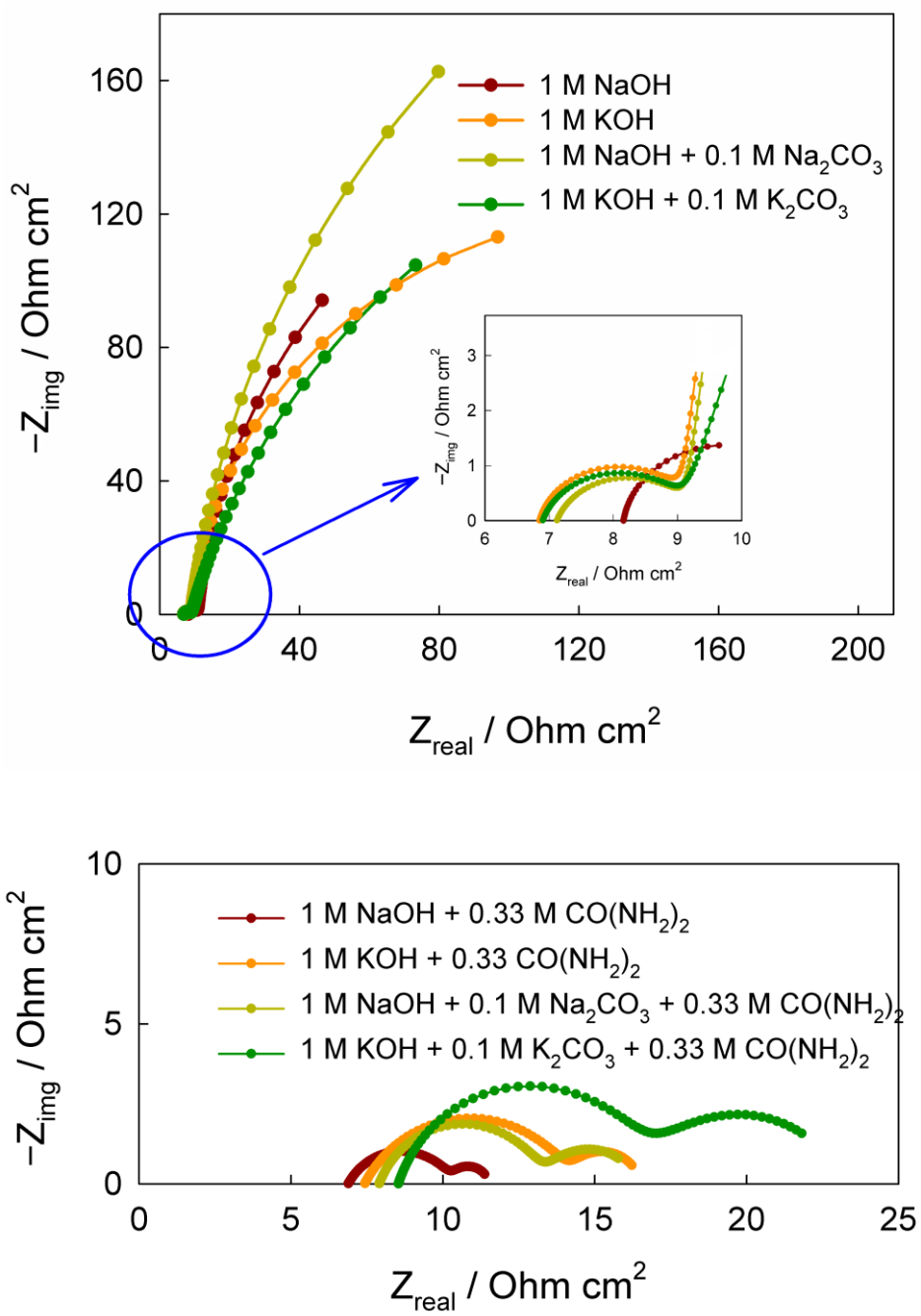

Figure 3. Nyquist plots recorded at a potential of 0.45 V in solutions of different compositions (as indicated in the figure).

In the low-frequency region, the second semicircle in the Nyquist diagrams (on the right side of the plot) for alkaline solutions without $CO(NH_2)_2$ has a considerably larger diameter than the first high-frequency semicircle, indicating a higher electrical resistance. This semicircle is likely associated with the adsorption of certain species, in particular hydroxide ions, on the electrode surface, which may participate in the electrochemical reaction. Since, within the frequency range used, the maximum of the imaginary part of the impedance for these semicircles could not be reached, the corresponding time constants were not determined. Nevertheless, a rough estimate suggests that these time constants probably exceed ~16 s. Regarding the second semicircle in the Nyquist plots for alkaline solutions containing $CO(NH_2)_2$, it corresponds to relatively large time constants (on the order of 3–4 s) with the corresponding characteristic frequencies of 0.03–0.05 Hz.

Table 2. Characteristic frequencies and time constants for electrochemical processes in solutions with different compositions.

Electrolyte Composition	High-Frequency Region		Low-Frequency Region	
	f_{peak}/Hz	τ/s	f_{peak}/Hz	τ/s
1 M NaOH	7.41	2.15×10^{-2}	–	–
1 M KOH	3.72	4.28×10^{-2}	–	–
1 M NaOH + 0.1 M Na_2CO_3	70.8	2.25×10^{-3}	–	–
1 M KOH + 0.1 M K_2CO_3	97.7	1.63×10^{-3}	–	–
1 M NaOH + 0.33 M $CO(NH_2)_2$	14.1	1.13×10^{-2}	0.0501	3.18
1 M KOH + 0.33 M $CO(NH_2)_2$	16.6	9.59×10^{-3}	0.0501	3.18
1 M NaOH + 0.33 M $CO(NH_2)_2$ + 0.1 M Na_2CO_3	16.6	9.59×10^{-3}	0.0363	4.38
1 M KOH + 0.33 M $CO(NH_2)_2$ + 0.1 M K_2CO_3	7.41	2.15×10^{-2}	0.0427	3.73

As is well known, a time constant reflects the characteristic relaxation time of a given electrochemical process to a new quasi-stationary state after a small external sinusoidal perturbation [59]. In this context, the magnitude of the time constant can, in a first approximation, be used to identify the nature of the electrochemical process. The similarity of time constants (and the corresponding characteristic frequencies) in the high-frequency region for solutions with and without urea suggests that they are likely caused by the same charge-transfer process in the $Ni(OH)_2 \leftrightarrow NiOOH$ redox reaction, which, in the case of added urea, is complicated by the indirect mechanism of its oxidation (reactions (4) and (6)). Regarding the second semicircle in the low-frequency region for solutions containing $CO(NH_2)_2$, it is reasonable to assume that oxidation proceeds via the direct mechanism (reactions (4) and (5)) involving adsorbed species, which accounts for the relatively long relaxation times [44].

It should be noted that changes in the time constant in EIS can be caused by multiple factors, including variations in charge-transfer resistance, interfacial capacitance, adsorption processes, and so on, which may occur simultaneously; therefore, such changes cannot be interpreted unambiguously [59]. For a more detailed and precise identification of the kinetics and mechanism of the investigated processes, a further analysis of Bode plots and modeling through the development of an equivalent circuit with the calculation of its individual quantitative parameters is required.

The obtained Bode plots for the DES-electrodeposited electrocatalyst in all eight investigated solutions exhibit a characteristic behavior, including a decrease in the impedance magnitude $|Z|$ with increasing frequency and the presence of two distinct phase-shift maxima (Figure 4). In the high-frequency region, $|Z|$ in all cases falls to values close to the ohmic resistance, while the phase approaches zero, indicating a negligible contribution from capacitive components. Two phase angle maxima, reflecting relaxation processes, are observed in the mid- and low-frequency ranges. In the low-frequency region, for solutions without urea, the phase maximum is well pronounced and reaches large values of ≈60–70°; by contrast, in urea-containing solutions, the phase peaks are substantially smaller, only ≈3–7°. This indicates a change in the mechanism from predominantly capacitive control to a mainly ohmic behavior, an acceleration of relaxation stages (shift in characteristic frequencies toward higher frequencies), and a modification of the double layer due to urea adsorption. Together, these factors render the system markedly less “RC-like”, manifested as a strong reduction in the phase angle maxima. In urea-containing solutions, the impedance magnitude $|Z|$ in the low-frequency range also increases substantially compared with solutions without urea, reflecting the influence of slow charge-transfer processes.

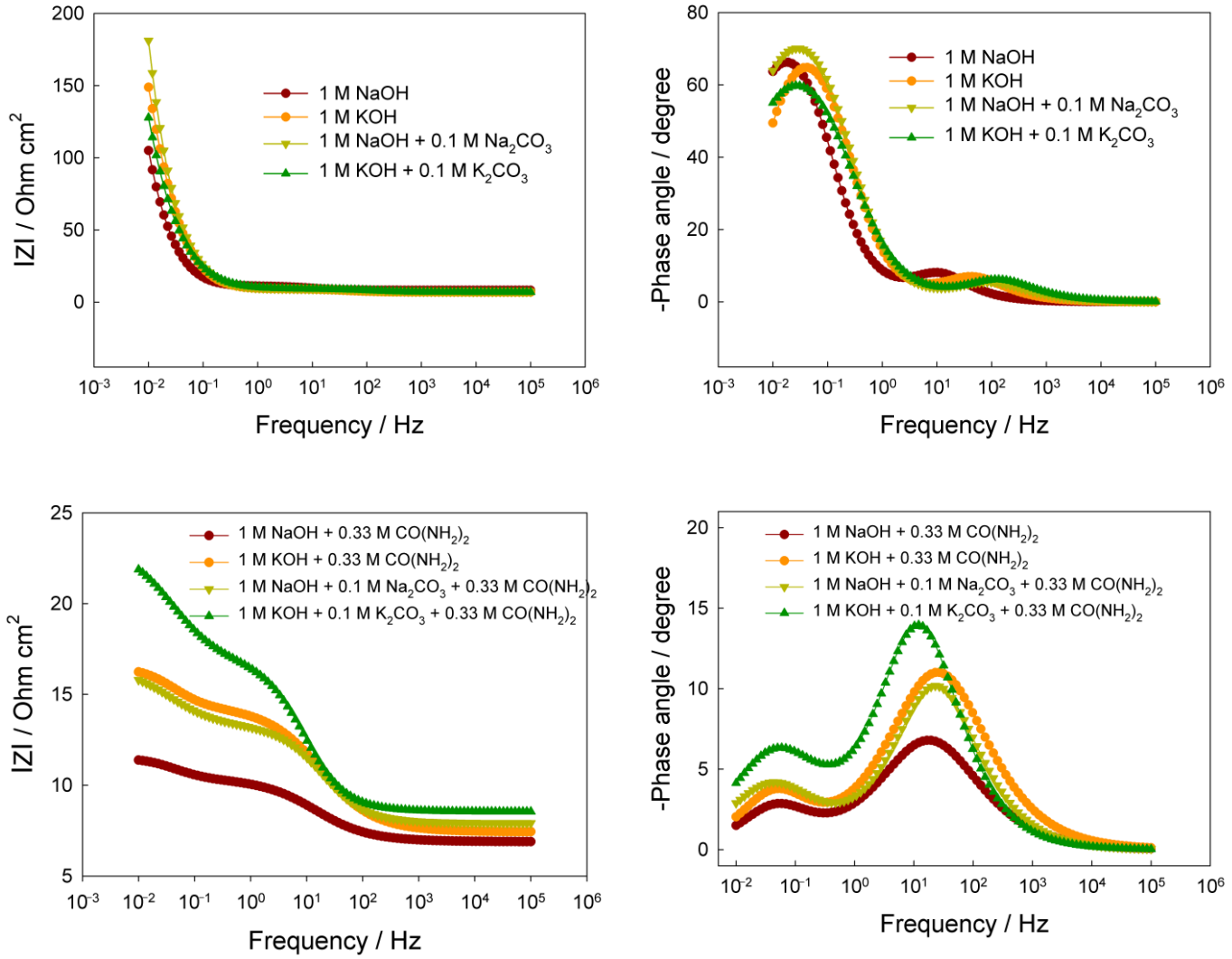

Figure 4. Bode plots recorded at a potential of 0.45 V in solutions of different compositions (as indicated in the figure).

A more detailed analysis of the phase angle peaks shows that in "pure" alkaline solutions (1 M NaOH or 1 M KOH), the maximum phase shift reaches 66.2° at 0.019 Hz and 64.8° at 0.0427 Hz, respectively. This indicates that the relaxation process proceeds faster in KOH, which is consistent with the higher mobility of K^+ and the potentially improved ion transport within the NiOOH layers. A similar trend is observed for systems containing carbonate ions: in 1 M NaOH + 0.1 M Na_2CO_3 the phase maximum is 70.1° at 0.0309 Hz, whereas in 1 M KOH + 0.1 M K_2CO_3 it is 59.8° at 0.0263 Hz. As seen, carbonate ions noticeably shift the phase angle maximum toward higher frequencies, suggesting the emergence of additional slow stages, most likely of adsorption-intercalation nature.

The introduction of urea fundamentally changes the system's behavior. In alkaline solutions containing $CO(NH_2)_2$, the phase angle maxima (at higher frequencies) become markedly lower: 6.8° at 16.6 Hz and 11.0° at 26.9 Hz for NaOH and KOH, respectively. Such a dramatic shift into the high-frequency region may indicate the emergence of rapid capacitance-controlled processes associated with the interaction of urea molecules with the surface of Ni-containing sites and with the modification of the interfacial layer at the atomic level. The phase shift decrease may also suggest partial destabilization or subtle structural changes in the NiOOH phase, making the surface reaction less "RC-like" and closer to the behavior of a system dominated by ohmic resistance.

The most complex frequency response is observed in mixed alkaline solutions containing both urea and carbonate ions. In these systems, the maximum phase shift reaches approximately 10.18° (22.9 Hz) and 13.95° (12.0 Hz). These values are intermediate between those of the pure "urea" and "carbonate" systems, yet they differ substantially in character: such parameters may indicate competition and mutual suppression between two types of processes, fast reactions involving $CO(NH_2)_2$ and slow surface rearrangements induced by CO_3^{2-}.

Interestingly, in the solutions containing urea, the impedance modulus |Z| exhibits several inflection points and changes in slope on the Bode plot, unlike the solutions without added urea. The presence of two nearly linear regions in the frequency dependence of the impedance modulus correlates well with the corresponding maxima in the phase angle vs. frequency relationships. Such behavior indicates a multiprocess system with several distinct mechanisms, each dominating within its own frequency range. These results are fully consistent with the Nyquist diagrams and confirm that the modification of electrolyte composition is an effective tool for controlling electrode kinetics and the behavior of electrocatalysts in the urea oxidation reaction.

Based on the analysis of the features of the Nyquist and Bode plots, an equivalent circuit (Figure 5), also known in the literature as the Armstrong–Henderson equivalent circuit [59,60], was proposed. This circuit has been previously used to interpret EIS measurements on oxidized nickel surfaces [61,62], including for the UOR occurring on such surfaces [44,63–65]. The equivalent circuit consists of the following elements:

(1) The ohmic resistance of the solution (R_S), which is localized in the electrolyte layer between the working electrode and the reference electrode. This parameter depends on the conductivity of the solution and the specific geometry of the electrochemical cell and therefore does not characterize the kinetics of the studied electrochemical system;

(2) An RC-like component consisting of a constant phase element (CPE_1) connected in parallel with a polarization resistance (R_{P1});

(3) An additional RC-like component consisting of a constant phase element (CPE_2) connected in parallel with a polarization resistance (R_{P2}), which is placed in series with R_{P1} in the electrical circuit.

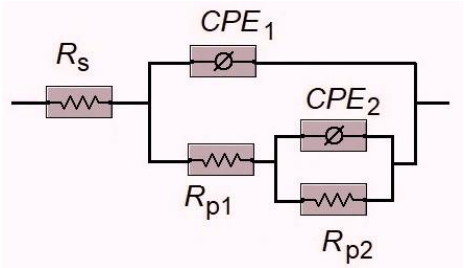

Figure 5. Equivalent circuit used for modeling the electrochemical impedance spectra.

It is worth noting that the polarization resistance $R_{P1(2)}$ is typically associated with resistive behavior and corresponds to the electrochemical impedance according to the following Equation:

$$R_p = \lim_{\omega \to 0} Z_{real} \quad (8)$$

where Z_{real} is the real part of complex faradaic impedance value extrapolated to zero frequency.

The need to incorporate constant phase elements (CPEs) instead of "ideal" capacitive elements in the equivalent circuit is related to the geometric and energetic heterogeneity of the electrode surface [66,67] and is diagnostically evident from the fact that the semicircles on the Nyquist plots are depressed (Figure 3). Surface heterogeneity causes an uneven distribution of various properties across the electrode, such as surface capacitance, polar-

ization resistance, and current distribution. As a result, the solid electrode surface deviates from the behavior of an ideal capacitor, for which the phase shift equals exactly –90°. The impedance of a constant phase element is usually described by the following Equation:

$$Z_{CPE} = \frac{1}{Y(j\omega)^n} \quad (9)$$

where Y is a parameter reflecting the capacitive behavior (non-ideal capacitor) with units of $Ohm^{-1}\ s^n\ cm^{-2}$ (or $F\ s^{n-1}\ cm^{-2}$); $j = \sqrt{-1}$ is the imaginary unit; $\omega = 2\pi f$ is the angular frequency in rad s^{-1} with f being the frequency in hertz; and n is a dimensionless empirical constant characterizing the phase deviation.

The value of n can, in principle, vary from 0 to 1, determining the phase deviation as $–90° \times n$. If $n = 1$, the electrode behaves as an ideal capacitor. If $n < 1$, the phase deviation is less than 90° (in magnitude), indicating the presence of a constant phase element. The more heterogeneous the electrode surface becomes, the more n deviates from unity [58,59], which is manifested as depressed (flattened) semicircles on the Nyquist plots.

In the employed equivalent circuit, the components R_{P1} and CPE_1 correspond to the high-frequency region of the electrochemical impedance spectrum (i.e., the left semicircle in the plots of Figure 3), whereas R_{P2} and CPE_2 are associated with the low-frequency region of the spectrum (i.e., the right semicircle in Figure 3). From the above, it follows that the R_{P1} and CPE_1 elements of the equivalent circuit reflect the kinetic characteristics of the charge transfer process in the $Ni(OH)_2 \leftrightarrow NiOOH$ redox reaction in alkaline media, whereas in solutions containing urea, they characterize the *indirect* mechanism of urea oxidation. On the other hand, the R_{P2} and CPE_2 elements (at lower frequencies) are responsible for adsorption processes on the nickel hydroxide surface in solutions without added $CO(NH_2)_2$ and, in urea-containing solutions, represent the kinetics of the *direct* urea oxidation mechanism.

It should be stressed that the distinction between the two resistive elements in the equivalent circuit follows from their characteristic time constants and potential-dependent behavior. R_{P1} dominates in the high-to-mid frequency region and evolves in parallel with the Ni(II)/Ni(III) redox transition, which is consistent with the fast charge-transfer step of the indirect, NiOOH-mediated UOR route. In contrast, R_{P2} appears in the low-frequency domain and becomes significant exclusively in urea-containing solutions after NiOOH is formed, which agrees with slower adsorption-controlled processes associated with the direct urea oxidation pathway. This separation of frequency domains and their potential dependence provides a consistent basis for assigning R_{P1} to the indirect and R_{P2} to the direct oxidation routes, respectively.

The quantitative parameters of the individual elements of the adapted equivalent circuit, calculated using the Gamry Elchem Analyst software package, are summarized in Table 3.

The obtained equivalent circuit parameters allow a quantitative assessment of the contribution of individual stages of the electrode processes to the overall impedance response. In particular, the values of the ohmic resistance R_S for all studied solutions range from approximately 6.8 to 8.5 Ω, confirming the absence of significant changes in the conductivity of the medium or the geometry of the cell. A slight tendency toward lower R_S values in KOH compared to NaOH is consistent with the somewhat higher ionic mobility of potassium ions; however, this effect is minor and does not determine the kinetics of the surface processes.

Table 3. Calculated parameters of electrochemical impedance for electrochemical processes in solutions with various compositions.

Electrolyte Composition	R_S/Ohm	R_{P1}/Ohm cm^2	CPE_1		R_{P2}/Ohm cm^2	CPE_2	
			Y_1/Ohm^{-1} s^{n1} cm^{-2}	n_1		Y_2/Ohm^{-1} s^{n2} cm^{-2}	n_2
1 M NaOH	8.16	3.11	8.36×10^{-3}	0.91	363.46	0.120	0.95
1 M KOH	6.85	2.41	3.80×10^{-3}	0.86	262.87	0.072	0.95
1 M NaOH + 0.1 M Na_2CO_3	7.12	2.16	3.49×10^{-3}	0.79	598.84	0.065	0.94
1 M KOH + 0.1 M K_2CO_3	6.90	2.31	2.15×10^{-3}	0.81	405.18	0.071	0.84
1 M NaOH + 0.33 M $CO(NH_2)_2$	6.89	3.49	14.82×10^{-3}	0.67	1.16	2.57	0.86
1 M KOH + 0.33 M $CO(NH_2)_2$	7.43	6.91	6.40×10^{-3}	0.68	2.20	1.43	0.86
1 M NaOH + 0.33 M $CO(NH_2)_2$ + 0.1 M Na_2CO_3	7.91	5.47	5.32×10^{-3}	0.76	3.08	1.00	0.74
1 M KOH + 0.33 M $CO(NH_2)_2$ + 0.1 M K_2CO_3	8.54	8.44	5.43×10^{-3}	0.79	6.23	0.46	0.72

The behavior of the high-frequency block elements (R_{P1} and CPE_1) is considerably more indicative. In "pure" alkaline solutions, the polarization resistance R_{P1} is lower in KOH than in NaOH, indicating faster charge transfer and more facile primary redox transformations in the $Ni(OH)_2$/NiOOH system. The addition of carbonate further decreases R_{P1} in both systems, which may suggest a certain modification of the surface hydroxide phases or a change in the local structure of the double layer, facilitating the involved electron-ion transfers. In contrast, the introduction of urea has a fundamentally different effect: in NaOH, its presence only slightly increases R_{P1}, whereas in KOH, R_{P1} rises sharply—almost threefold compared to pure KOH. This difference indicates that the interaction of urea with the active NiOOH sites strongly depends on the nature of the cation. It is likely that in KOH, adsorption or partial complexation of urea with the active surface sites leads to stronger blockage of the electrode surface, particularly in regions where fast charge transfer processes occur.

The CPE_1 parameters support this conclusion. In "pure" alkaline solutions, the n_1 values are close to ≈0.9, indicating pseudo-capacitive behavior approaching ideality and a relatively structurally homogeneous surface. In the presence of urea, n_1 decreases to ≈0.67–0.68, regardless of the cation, reflecting increased heterogeneity of the surface states and the emergence of a more distributed pseudo-capacitance, likely due to the formation of a heterogeneous layer of adsorbed UOR intermediate products or partial restructuring of the NiOOH surface oxide. The increase in the capacitance parameter Y_1 (especially in the NaOH + urea solution) may correspond to the accumulation of surface intermediates and an increase in the effective pseudo-capacitance at high frequencies.

The behavior of the low-frequency block, which represents the slow stages associated with adsorption phenomena and the direct pathway of urea oxidation, is entirely different. In "pure" NaOH and KOH solutions, the R_{P2} values are very high (mostly hundreds of Ω cm^2), reflecting extremely slow electrochemical rearrangements within the hydroxide film. Notably, carbonate ions significantly increase R_{P2} (most markedly in NaOH), indicating strong inhibition of the slow stages, likely due to CO_3^{2-} adsorption on NiOOH or incorporation of carbonate into the hydroxide-oxide structure. In contrast, urea induces a radically different effect: in NaOH + urea and KOH + urea solutions, R_{P2} sharply decreases to values on the order of a few Ω cm^2. This behavior indicates a substantial facilitation of the processes dominating the low-frequency range and is consistent with the rapid oxidation of urea on NiOOH via direct mechanism when a sufficient number of surface active sites are available. Together with the increase in Y_2 in these systems, this suggests

the formation of a large number of adsorbed intermediate species and the activation of the pseudo-capacitive component, reflecting the multistep nature of UOR.

The combined effect of urea and carbonates is particularly noteworthy. In such systems, R_{P2} rises to intermediate values, while the CPE_2 parameters remain elevated, indicating a competitive adsorption between urea and carbonate on the NiOOH surface sites. Consequently, the presence of carbonate partially counteracts the activating effect of urea in the low-frequency range, which is consistent with the reported blocking role of carbonates in alkaline Ni–UOR systems.

Thus, the analysis of the equivalent circuit model clearly demonstrates the distinct contributions of the individual solution components. Potassium ions accelerate the high-frequency charge-transfer processes in the $Ni(OH)_2$/NiOOH system, whereas urea strongly activates the low-frequency pathway associated with the direct mechanism of UOR. Carbonate ions, in contrast, inhibit processes in the low-frequency range, and in combined systems (simultaneous presence of $CO(NH_2)_2$ and CO_3^{2-}), their effect competes with the activating influence of urea. The observed trends are consistent with the Bode plot behavior (Figure 4) and CVA analysis (Figures 1 and 2), confirming that the electrode kinetics in Ni–urea systems are governed by the balance between fast surface NiOOH redox processes and slower adsorption-catalytic steps, which are sensitive to the nature of the electrolyte.

From a practical perspective, the obtained results are important for optimizing electrolytes intended for water electrolysis involving the urea oxidation process. In conventional alkaline electrolyzers operating via the HER/OER scheme, potassium hydroxide solutions are generally considered more favorable due to their higher ionic conductivity, which reduces the cell voltage and lowers energy consumption. However, in systems where urea oxidation replaces the oxygen evolution reaction, our results reveal a different scenario. In particular, the equivalent circuit parameters indicate that in NaOH + urea, R_{P1} values increase only slightly, whereas R_{P2} drops sharply to a few ohm cm^2, reflecting the effective activation of the low-frequency channel of electrochemical transformations and accelerated progression of the key UOR steps. This suggests that in sodium-based electrolytes, urea does not block active sites in the high-frequency regime, while simultaneously significantly enhancing the direct oxidation mechanism.

In contrast, in KOH + urea, a pronounced increase in R_{P1} is observed, indicating inhibition of the fast NiOOH redox processes at the initial stages, while the increase in structural heterogeneity (decrease in n_1) points to stronger disorganization of the surface layer. This effect may be associated with the specific interaction of K^+ with hydrated urea molecules and surface Ni-containing sites. As noted above, K^+ ions significantly influence the structure of the aqueous environment and the stability of adsorbed OH^-; in the presence of organic molecules, it can form more stable solvation-adsorption clusters that hinder the progression of fast charge-transfer steps. Therefore, for UOR systems, sodium-based alkaline media prove to be a more effective matrix, providing an optimal balance between the availability of surface NiOOH active sites and sufficient hydration to facilitate the urea oxidation pathway.

Equally important is the effect of carbonate accumulation. In practical electrolyzers operating over extended periods with urea, carbonate content inevitably builds up due to the chemical and electrochemical decomposition of $CO(NH_2)_2$ molecules. Our results clearly demonstrate that the presence of CO_3^{2-} substantially increases the low-frequency resistance R_{P2} (especially in KOH), hindering the slow stages and effectively "closing" the catalytic channel that would otherwise be available for UOR in purely alkaline solutions. This behavior is consistent with the probable intercalation or strong adsorption of carbonates on NiOOH phases, which limits hydroxide mobility and blocks reactive sites. In systems containing both urea and carbonate, competitive adsorption likely occurs, partially

mitigating the activating effect of urea and indirectly highlighting the importance of controlling CO_3^{2-} concentration in the electrolyte. These findings also indicate that the gradual in situ generation and accumulation of carbonate, and its influence on catalyst stability and UOR kinetics during prolonged operation, should be addressed in future studies, including long-term experiments coupled with operando monitoring of carbonate speciation.

For practical electrolysis, this implies that carbonate accumulation is undesirable, as it gradually decreases UOR efficiency and promotes a return to kinetics characteristic of the slower OER. This can be mitigated through several approaches: periodic electrolyte regeneration (partial or complete replacement), maintaining a low-CO_2 protective atmosphere, carbonate removal via precipitation (e.g., with $Ca(OH)_2$ or $Ba(OH)_2$), and optimizing the anode potential and hydrodynamic conditions to limit carbonate buildup. In long-term industrial processes, a two-pronged strategy may be most effective: employing NaOH as the primary electrolyte and performing periodic carbonate removal, which would help sustain high UOR rates while preventing catalytic activity degradation.

In a broader context, the obtained results demonstrate that the choice of electrolyte for UOR cannot be based solely on criteria established for conventional OER electrolysis. Interactions among the cation, the organic substrate molecule, and the surface NiOOH phases are complex, revealing that sodium-based media provide a more favorable combination of kinetics and stability, whereas potassium-based systems, although effective for OER, exhibit impaired performance under UOR conditions. Similarly, carbonate ions, which are often considered inert in OER systems, show a clearly detrimental effect in UOR. This highlights the need for specifically optimized electrolytes for urea-assisted hydrogen systems and opens opportunities for further research on additives that could selectively suppress carbonate adsorption or, conversely, stabilize favorable surface electrocatalytic sites.

4. Conclusions

The conducted study demonstrated that the addition of urea significantly changes the electrochemical behavior of the nickel hydroxide electrode in alkaline media and transforms the frequency structure of the impedance response. Modeling using the Armstrong–Henderson equivalent circuit shows that in sodium-based solutions, urea sharply decreases the low-frequency polarization resistance and enhances the pseudo-capacitive response, indicating effective activation of the slow adsorption-catalytic stages of UOR. In contrast, in potassium-based solutions, urea substantially increases the high-frequency polarization resistance and disrupts the uniformity of the surface structure, reflecting inhibition of the primary $Ni(OH)_2 \leftrightarrow NiOOH$ redox transformations.

Comparison of NaOH and KOH reveals that, although KOH is generally considered more efficient for conventional alkaline water electrolysis, sodium electrolytes provide more favorable kinetics in systems involving UOR due to a better balance between the accessibility of NiOOH active sites and the rates of key reaction steps.

The pronounced detrimental effect of carbonate ions, which increase polarization resistance and partially block surface sites, highlights the need to control their accumulation in long-term electrolyzers. Desirable strategies include periodic electrolyte renewal, minimizing CO_2 exposure, and/or employing chemical carbonate removal methods. The obtained results provide clear guidance for optimizing the composition of alkaline electrolytes in urea-assisted systems for green hydrogen production and can be applied in the development of energy-efficient anodic processes that combine the advantages of alkaline electrolysis with organic compound oxidation.

Author Contributions: Conceptualization, V.S.P.; methodology, V.S.P.; formal analysis, V.S.P., D.A.S. and O.D.S.; investigation, D.A.S. and O.D.S.; visualization, V.S.P., D.A.S. and O.D.S.; funding acquisition, V.S.P.; writing—original draft, V.S.P.; writing—review and editing, V.S.P. All authors have read and agreed to the published version of the manuscript.

Funding: This research was funded by the Ministry of Education and Science of Ukraine, grant number 0124U000563.

Data Availability Statement: The data presented in this study are available upon request from the corresponding author. The data are not publicly available due to technical limitations.

Conflicts of Interest: The authors declare no conflicts of interest. The funder had no role in the design of the study; in the collection, analyses, or interpretation of data; in the writing of the manuscript; or in the decision to publish the results.

Abbreviations

The following abbreviations are used in this manuscript:

HER	Hydrogen evolution reaction
OER	Oxygen evolution reaction
UOR	Urea oxidation reaction
DES	Deep eutectic solvent
EIS	Electrochemical impedance spectroscopy
CVA	Cyclic voltammogram
CPE	Constant phase element
CAS	Chemical Abstracts Service (registry number)

References

1. Dawood, F.; Anda, M.; Shafiullah, G.M. Hydrogen production for energy: An overview. *Int. J. Hydrogen Energy* **2020**, *45*, 3847–3869. [CrossRef]
2. Squadrito, G.; Maggio, G.; Nicita, A. The green hydrogen revolution. *Renew. Energy* **2023**, *216*, 119041. [CrossRef]
3. Jeje, S.O.; Marazani, T.; Obiko, J.O.; Shongwe, M.B. Advancing the hydrogen production economy: A comprehensive review of technologies, sustainability, and future prospects. *Int. J. Hydrogen Energy* **2024**, *78*, 642–661. [CrossRef]
4. Ansari, S.A.; Alam, M.W.; Dhanda, N.; Abbasi, M.S.; Ahmed, M.E.; Bader Alrashidi, A.; Al-Farhan, A.M.; Abebe, B. Sustainable hydrogen production, a review of methods, types, applications, challenges, and future perspectives. *Glob. Chall.* **2025**, *9*, 2500086. [CrossRef]
5. Okada, Y.; Sasaki, E.; Watanabe, E.; Hyodo, S.; Nishijima, H. Development of dehydrogenation catalyst for hydrogen generation in organic chemical hydride method. *Int. J. Hydrogen Energy* **2006**, *31*, 1348–1356. [CrossRef]
6. Diglio, M.; Contento, I.; Impemba, S.; Berretti, E.; Della Sala, P.; Oliva, G.; Naddeo, V.; Caporali, S.; Primo, A.; Talotta, C.; et al. Hydrogen production from formic acid decomposition promoted by gold nanoparticles supported on a porous polymer matrix. *Energy Fuels* **2025**, *39*, 14320–14329. [CrossRef]
7. Adhikari, S.P.; Hood, Z.D.; Lachgar, A. Semiconductor heterojunctions for enhanced visible light photocatalytic H_2 production. *MRS Adv.* **2018**, *3*, 3263–3270. [CrossRef]
8. Bahadoran, A.; Liu, Q.; Ramakrishna, S.; Sadeghi, B.; De Castro, M.M.; Cavaliere, P.D. Hydrogen production as a clean energy carrier through heterojunction semiconductors for environmental remediation. *Energies* **2022**, *15*, 3222. [CrossRef]
9. Impemba, S.; Provinciali, G.; Filippi, J.; Salvatici, C.; Berretti, E.; Caporali, S.; Banchelli, M.; Caporali, M. Engineering the heterojunction between TiO_2 and In_2O_3 for improving the solar-driven hydrogen production. *Int. J. Hydrogen Energy* **2024**, *63*, 896–904. [CrossRef]
10. Boddula, R.; Lee, Y.-Y.; Masimukku, S.; Chang-Chien, G.-P.; Pothu, R.; Srivastava, R.K.; Sarangi, P.K.; Selvaraj, M.; Basumatary, S.; Al-Qahtani, N. Sustainable hydrogen production: Solar-powered biomass conversion explored through (Photo)electrochemical advancements. *Process Saf. Environ. Prot.* **2024**, *186*, 1149–1168. [CrossRef]
11. Pan, H.; Li, J.; Wang, Y.; Xia, Q.; Qiu, L.; Zhou, B. Solar-driven biomass reforming for hydrogen generation: Principles, advances, and challenges. *Adv. Sci.* **2024**, *11*, 2402651. [CrossRef]
12. Impemba, S.; Provinciali, G.; Filippi, J.; Caporali, S.; Muzzi, B.; Casini, A.; Caporali, M. Tightly interfaced Cu_2O with In_2O_3 to promote hydrogen evolution in presence of biomass-derived alcohols. *ChemNanoMat* **2024**, *10*, e202400459. [CrossRef]

13. Vidas, L.; Castro, R. Recent developments on hydrogen production technologies: State-of-the-art review with focus on green-electrolysis. *Appl. Sci.* **2021**, *11*, 11363. [CrossRef]
14. Ajanovic, A.; Sayer, M.; Haas, R. The economics and the environmental benignity of different colors of hydrogen. *Int. J. Hydrogen Energy* **2022**, *47*, 24136. [CrossRef]
15. Shih, A.J.; Monteiro, M.C.O.; Dattila, F.; Pavesi, D.; Philips, M.; da Silva, A.H.M.; Vos, R.E.; Ojha, K.; Park, S.; van der Heijden, O.; et al. Water electrolysis. *Nat. Rev. Methods Primers* **2022**, *2*, 84. [CrossRef]
16. Raveendran, A.; Chandran, M.; Dhanusuraman, R. A comprehensive review on the electrochemical parameters and recent material development of electrochemical water splitting electrocatalysts. *RSC Adv.* **2023**, *13*, 3843–3876. [CrossRef] [PubMed]
17. Zhou, W.; Chen, S.; Meng, X.; Li, J.; Gao, J. Energy-saving cathodic H_2 production enabled by non-oxygen evolution anodic reactions: A critical review on fundamental principles and applications. *Int. J. Hydrogen Energy* **2023**, *48*, 15748–15770. [CrossRef]
18. Boggs, B.K.; King, R.L.; Botte, G.G. Urea electrolysis: Direct hydrogen production from urine. *Chem. Commun.* **2009**, *32*, 4859–4861. [CrossRef]
19. Sun, X.; Ding, R. Recent progress with electrocatalysts for urea electrolysis in alkaline media for energy-saving hydrogen production. *Catal. Sci. Technol.* **2020**, *10*, 1567–1581. [CrossRef]
20. Yang, K.; Hao, L.; Hou, Y.; Zhang, J.; Yang, J.H. Summary and application of Ni-based catalysts for electrocatalytic urea oxidation. *Int. J. Hydrogen Energy* **2024**, *51*, 966–981. [CrossRef]
21. Paygozar, S.; Aghdam, A.S.R.; Hassanizadeh, E.; Andaveh, R.; Darband, G.B. Recent progress in non-noble metal-based electrocatalysts for urea-assisted electrochemical hydrogen production. *Int. J. Hydrogen Energy* **2023**, *48*, 7219–7259. [CrossRef]
22. Anuratha, K.S.; Rinawati, M.; Wu, T.H.; Yeh, M.H.; Lin, J.Y. Recent development of nickel-based electrocatalysts for urea electrolysis in alkaline solution. *Nanomaterials* **2022**, *12*, 2970. [CrossRef] [PubMed]
23. Akkari, S.; Sánchez-Sánchez, C.M.; Hopsort, G.; Serrano, K.G.; Loubière, K.; Tzedakis, T.; Benyahia, R.; Rebiai, L.; Bastide, S.; Cachet-Vivier, C.; et al. Progress on electrochemical and photoelectrochemical urea and ammonia conversion from urine for sustainable wastewater treatment. *Appl. Catal. B Environ. Energy* **2025**, *362*, 124718. [CrossRef]
24. Gao, X.; Zhang, S.; Wang, P.; Jaroniec, M.; Zheng, Y.; Qiao, S.-Z. Urea catalytic oxidation for energy and environmental applications. *Chem. Soc. Rev.* **2024**, *53*, 1552–1591. [CrossRef] [PubMed]
25. Weerakoon, D.; Bansal, B.; Padhye, L.P.; Rachmani, A.; Wright, L.J.; Roberts, G.S.; Baroutian, S. A critical review on current urea removal technologies from water: An approach for pollution prevention and resource recovery. *Sep. Purif. Technol.* **2023**, *314*, 123652. [CrossRef]
26. Swify, S.; Mažeika, R.; Baltrusaitis, J.; Drapanauskaitė, D.; Barčauskaitė, K. Review: Modified urea fertilizers and their effects on improving nitrogen use efficiency (NUE). *Sustainability* **2024**, *16*, 188. [CrossRef]
27. Knospe, P.; Shams Uldeen, M.; Reichmann, R.; Seithümmer, J.; Abdulkarim, A.; Rubbert, L.V.; Knospe, F.; Dornbusch, M. Next-generation urea resins: Formaldehyde-free coating materials based on higher aldehydes and amides. *J. Coat. Technol. Res.* **2025**, *22*, 999–1017. [CrossRef]
28. Ghosh, A.K.; Brindisi, M. Urea derivatives in modern drug discovery and medicinal chemistry. *J. Med. Chem.* **2020**, *63*, 2751–2788. [CrossRef]
29. Protsenko, V.S. Thermodynamic aspects of urea oxidation reaction in the context of hydrogen production by electrolysis. *Int. J. Hydrogen Energy* **2023**, *48*, 24207–24211. [CrossRef]
30. Protsenko, V.S.; Bobrova, L.S.; Butyrina, T.E.; Sukhatskyi, O.D. Thermodynamics of electrochemical urea oxidation reaction coupled with cathodic hydrogen evolution reaction in an alkaline solution: Effect of carbonate formation. *Int. J. Hydrogen Energy* **2024**, *59*, 354–358. [CrossRef]
31. Protsenko, V. Towards sustainable urea electro-oxidation: A thermodynamic and green chemistry evaluation of alternative pathways. *R. Soc. Open Sci.* **2025**, *12*, 250156. [CrossRef]
32. Wang, H.; Zheng, X.; Fang, L.; Lu, S. Urea electrooxidation in alkaline environment: Fundamentals and applications. *ChemElectroChem* **2023**, *10*, e202300138. [CrossRef]
33. Protsenko, V.S.; Shaiderov, D.A.; Sukhatskyi, O.D.; Butyrina, T.E.; Korniy, S.A. Nickel-containing electrocatalysts for green hydrogen production: Electrodeposition from deep eutectic solvent-based solutions and electrocatalytic activity for hydrogen evolution, oxygen evolution and urea oxidation reactions. *J. Appl. Electrochem.* **2025**, *55*, 2129–2148. [CrossRef]
34. Kityk, A.; Pavlik, V.; Hnatko, M. Exploring deep eutectic solvents for the electrochemical and chemical synthesis of photo- and electrocatalysts for hydrogen evolution. *Int. J. Hydrogen Energy* **2023**, *48*, 39823–39853. [CrossRef]
35. Al-Farsi, R.; Hayyan, M. Deep eutectic solvents: Green multi-task agents for sustainable super green hydrogen technologies. *J. Energy Chem.* **2024**, *92*, 357–382. [CrossRef]
36. Hansen, B.B.; Spittle, S.; Chen, B.; Poe, D.; Zhang, Y.; Klein, J.M.; Horton, A.; Adhikari, L.; Zelovich, T.; Doherty, B.W.; et al. Deep eutectic solvents: A review of fundamentals and applications. *Chem. Rev.* **2021**, *121*, 1232–1285. [CrossRef]
37. Abbott, A.P. Deep eutectic solvents and their application in electrochemistry. *Curr. Opin. Green Sustain. Chem.* **2022**, *36*, 100649. [CrossRef]

38. Zhang, C.; Fu, Y.; Gao, W.; Bai, T.; Cao, T.; Jin, J.; Xin, B. Deep eutectic solvent-mediated electrocatalysts for water splitting. *Molecules* **2022**, *27*, 8098. [CrossRef]
39. Zhang, C.; Bai, T.; Sun, Y.; Xin, B.; Zhang, S. Ionic liquid/deep eutectic solvent-mediated Ni-based catalysts and their application in water splitting electrocatalysis. *Catalysts* **2022**, *12*, 928. [CrossRef]
40. Daramola, D.A.; Singh, D.; Botte, G.G. Dissociation rates of urea in the presence of NiOOH catalyst: A DFT analysis. *J. Phys. Chem. A* **2010**, *114*, 11513–11521. [CrossRef] [PubMed]
41. Vedharathinam, V.; Botte, G.G. Direct evidence of the mechanism for the electro-oxidation of urea on $Ni(OH)_2$ catalyst in alkaline medium. *Electrochim. Acta* **2013**, *108*, 660–665. [CrossRef]
42. Wang, D.; Botte, G.G. In situ X-ray diffraction study of urea electrolysis on nickel catalysts. *ECS Electrochem. Lett.* **2014**, *3*, H29–H32. [CrossRef]
43. Singh, R.K.; Rajavelu, K.; Montag, M.; Schechter, A. Advances in catalytic electrooxidation of urea: A review. *Energy Technol.* **2021**, *9*, 2100017. [CrossRef]
44. Guo, F.; Ye, K.; Du, M.; Huang, X.; Cheng, K.; Wang, G.; Cao, D. Electrochemical impedance analysis of urea electro-oxidation mechanism on nickel catalyst in alkaline medium. *Electrochim. Acta* **2016**, *210*, 474–482. [CrossRef]
45. Gebremariam, G.K.; Jovanović, A.Z.; Pašti, I.A. The effect of electrolytes on the kinetics of the hydrogen evolution reaction. *Hydrogen* **2023**, *4*, 776–806. [CrossRef]
46. Monteiro, M.C.O.; Goyal, A.; Moerland, P.; Koper, M.T.M. Understanding cation trends for hydrogen evolution on platinum and gold electrodes in alkaline media. *ACS Catal.* **2021**, *11*, 14328–14335. [CrossRef]
47. Li, P.; Jiang, Y.-L.; Men, Y.; Jiao, Y.-Z.; Chen, S. Kinetic cation effect in alkaline hydrogen electrocatalysis and double layer proton transfer. *Nat. Commun.* **2025**, *16*, 1844. [CrossRef]
48. Marcandalli, G.; Boterman, K.; Koper, M.T.M. Understanding hydrogen evolution reaction in bicarbonate buffer. *J. Catal.* **2022**, *405*, 346–354. [CrossRef]
49. Carr, J.K.; Buchanan, L.E.; Schmidt, J.R.; Zanni, M.T.; Skinner, J.L. Structure and dynamics of urea/water mixtures investigated by vibrational spectroscopy and molecular dynamics simulation. *J. Phys. Chem. B* **2013**, *117*, 13291–13300. [CrossRef]
50. Moll, C.J.; Versluis, J.; Bakker, H.J. Direct observation of the orientation of urea molecules at charged interfaces. *J. Phys. Chem. Lett.* **2021**, *12*, 10823–10828. [CrossRef]
51. del Rosario, J.A.D.; Li, G.; Labata, M.F.M.; Ocon, J.D.; Chuang, P.-Y.A. Unravelling the roles of alkali-metal cations for the enhanced oxygen evolution reaction in alkaline media. *Appl. Catal. B Environ.* **2021**, *288*, 119981. [CrossRef]
52. Mangel Raventos, A.; Kortlever, R. Effect of different alkali metal cations on the oxygen evolution activity and battery capacity of nickel electrodes in concentrated hydroxide electrolytes. *Electrochim. Acta* **2022**, *415*, 140255. [CrossRef]
53. Gallenberger, J.; Gohlke, C.; Neumann, M.; Mechler, A.K.; Hofmann, J.P. Water dissociation on NiOOH in alkaline water electrolysis improves with increasing alkali metal cation size. *ChemSusChem* **2025**, *18*, e202402596. [CrossRef]
54. Cha, S.; Cao, X.; Du, W.; Jin, H.; Liu, Y.; Wang, R.; Yang, Y.; Sun, B.; Yang, X.; Gong, M. The ion effect on electrocatalytic oxidation reactions. *J. Mater. Chem. A* **2024**, *12*, 32548–32565. [CrossRef]
55. Ghosh, S.; Dasgupta, B.; Kalra, S.; Ashton, M.L.P.; Yang, R.; Kueppers, C.J.; Gok, S.; Alonso, E.G.; Schmidt, J.; Laun, K.; et al. Evolution of carbonate-intercalated γ-NiOOH from a molecularly derived nickel sulfide (pre)catalyst for efficient water and selective organic oxidation. *Small* **2023**, *19*, 2206679. [CrossRef] [PubMed]
56. Hall, D.S.; Lockwood, D.J.; Bock, C.; MacDougall, B.R. Nickel hydroxides and related materials: A review of their structures, synthesis and properties. *Proc. R. Soc. A* **2015**, *471*, 20140792. [CrossRef] [PubMed]
57. Chen, Z.; Wei, W.; Shon, H.K.; Ni, B.-J. Designing bifunctional catalysts for urea electrolysis: Progress and perspectives. *Green Chem.* **2024**, *26*, 631–654. [CrossRef]
58. Lazanas, A.C.; Prodromidis, M.I. Electrochemical Impedance Spectroscopy—A Tutorial. *ACS Meas. Sci. Au* **2023**, *3*, 162–193. [CrossRef] [PubMed]
59. Barsoukov, E.; Macdonald, J.R. *Impedance Spectroscopy: Theory, Experiment, and Applications*, 2nd ed.; John Wiley & Sons: Hoboken, NJ, USA, 2005.
60. Armstrong, R.D.; Henderson, M. Impedance plane display of a reaction with an adsorbed intermediate. *J. Electroanal. Chem. Interf. Electrochem.* **1972**, *39*, 81–90. [CrossRef]
61. Lyons, M.E.G.; Brandon, M.P. The oxygen evolution reaction on passive oxide covered transition metal electrodes in aqueous alkaline solution. Part 1—Nickel. *Int. J. Electrochem. Sci.* **2008**, *3*, 1386–1424. [CrossRef]
62. Protsenko, V.S.; Butyrina, T.E.; Danilov, F.I. Kinetics and mechanism of electrochemical oxygen evolution in an alkaline solution on nickel coatings. *J. Chem. Technol.* **2022**, *30*, 26–33. [CrossRef]
63. Mohamed, I.M.A.; Kanagaraj, P.; Yasin, A.S.; Iqbal, W.; Liu, C. Electrochemical impedance investigation of urea oxidation in alkaline media based on electrospun nanofibers towards the technology of direct-urea fuel cells. *J. Alloys Compd.* **2020**, *816*, 152513. [CrossRef]

64. Yang, M.; Liu, Z.; Liu, F.; Lv, Y.; Zhang, J. Boosting electrocatalytic urea oxidation performance of NiS_x-VS_4-C mediated via glycerol coking. *J. Alloys Compd.* **2024**, *1008*, 176743. [CrossRef]
65. Upadhyay, P.; Deka, A.; Chakma, S. Unlocking efficient electrochemical urea oxidation and understanding mechanism insights of Co-doped NiS. *ACS Eng. Au* **2025**, *5*, 450–467. [CrossRef]
66. Mulder, W.H.; Sluyters, J.H. An explanation of depressed semi-circular arcs in impedance plots for irreversible electrode reactions. *Electrochim. Acta* **1988**, *33*, 303–310. [CrossRef]
67. Rammelt, U.; Reinhard, G. On the applicability of a constant phase element (CPE) to the estimation of roughness of solid metal electrodes. *Electrochim. Acta* **1990**, *35*, 1045–1049. [CrossRef]